Electronic Supplementary Material (ESI) for Energy Advances.

Supporting Information

Cation Synergy in Sr and Al substituted $LaMnO_3$ during Solar Thermochemical CO_2 Splitting

*Mahesh Muraleedharan Nair and Stéphane Abanades**

Processes, Materials and Solar Energy Laboratory, PROMES-CNRS (UPR 8521), 7 Rue du Four Solaire, 66120 Font-Romeu, France

Email: Stephane.Abanades@promes.cnrs.fr

Figures

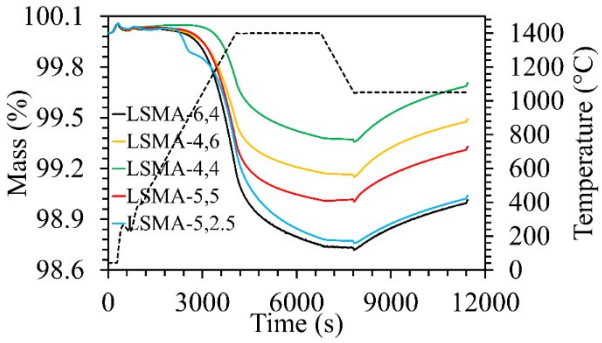

Figure S1. Mass variation profiles of $La_xSr_{1-x}Mn_yAl_{1-y}O_3$ perovskite oxygen carriers during one redox cycle comprising thermochemical reduction and subsequent CO_2 splitting. The dashed line represents the corresponding temperature variation.

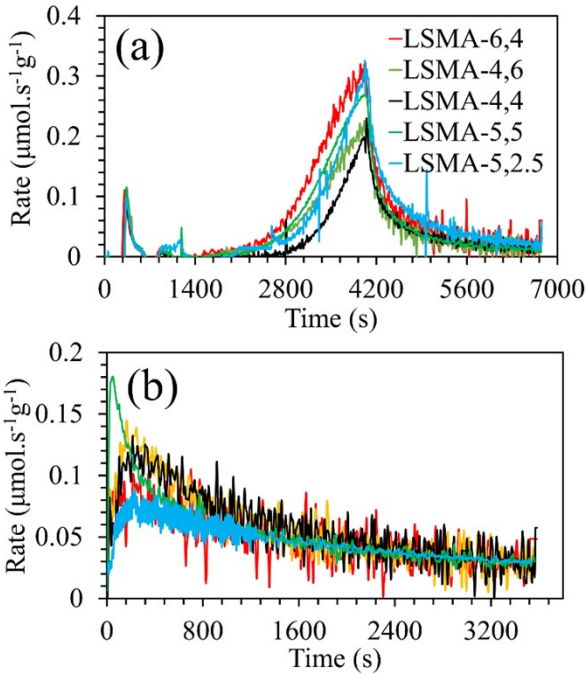

Figure S2. Reaction rates for (a) O_2 evolution and (b) CO evolution derived from mass variation during thermochemical reduction and CO_2-induced re-oxidation of $La_xSr_{1-x}Mn_yAl_{1-y}O_3$.

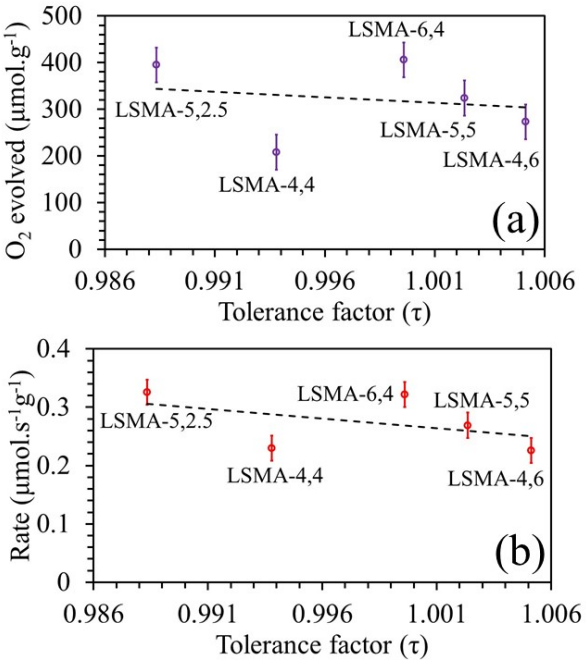

Figure S3. Amounts of O_2 evolved (a) and reduction rates (b) as a function of tolerance factor for $La_xSr_{1-x}Mn_yAl_{1-y}O_3$ oxygen carriers.

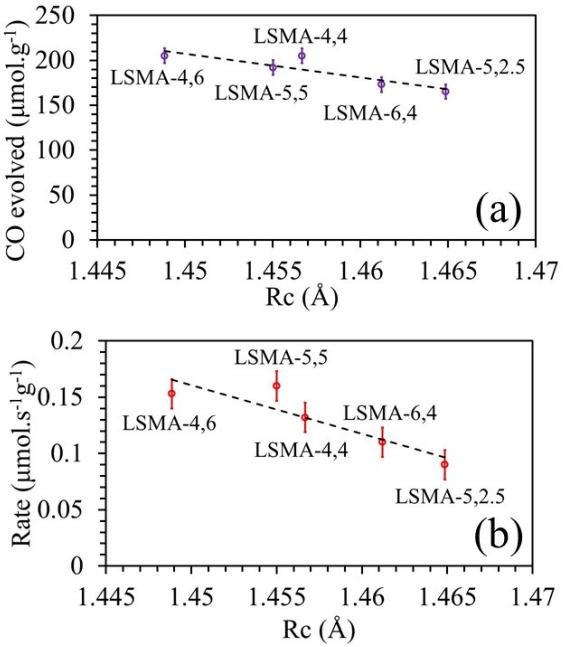

Figure S4. Amounts of CO evolved (a) and re-oxidation rates (b) as a function of critical radius for $La_xSr_{1-x}Mn_yAl_{1-y}O_3$ oxygen carriers.

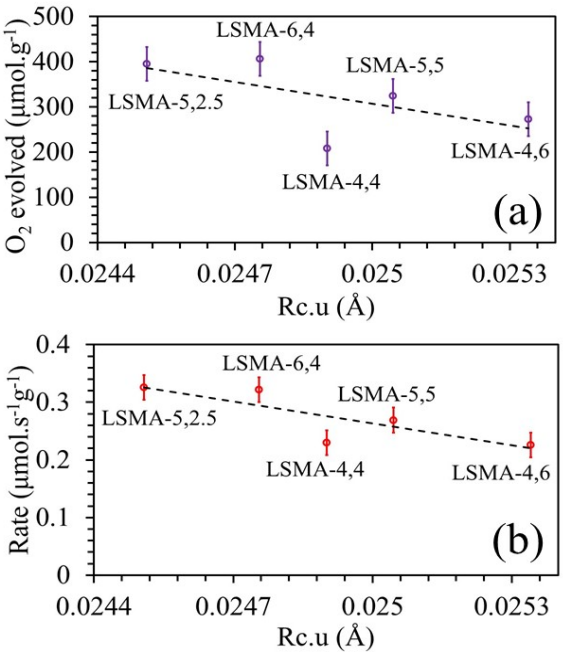

Figure S5. Amounts of O_2 evolved (a) and reduction rates (b) as a function of critical radius per unit cell volume for a series of $La_xSr_{1-x}Mn_yAl_{1-y}O_3$ oxygen carriers.

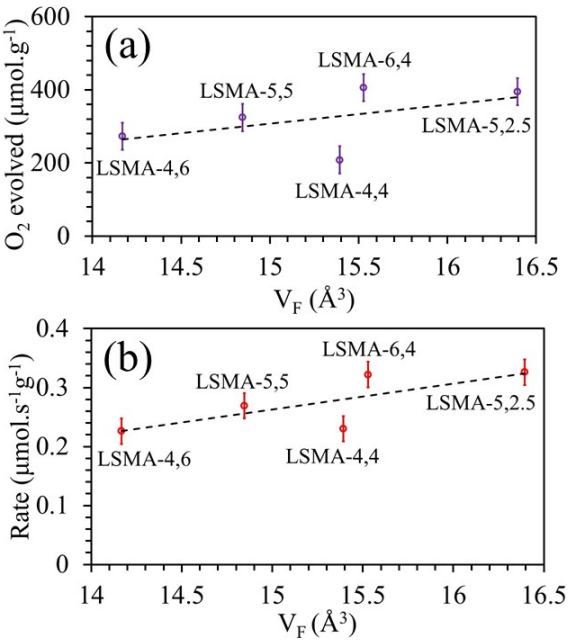

Figure S6. Amounts of O_2 evolved (a) and reduction rates (b) as a function of lattice free volumes for $La_xSr_{1-x}Mn_yAl_{1-y}O_3$ oxygen carriers.

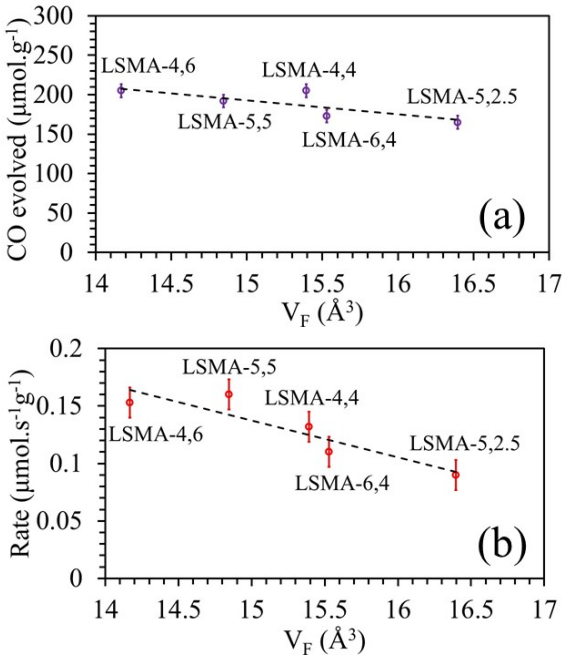

Figure S7. Amounts of CO evolved (a) and re-oxidation rates (b) as a function of lattice free volumes for $La_xSr_{1-x}Mn_yAl_{1-y}O_3$ oxygen carriers.

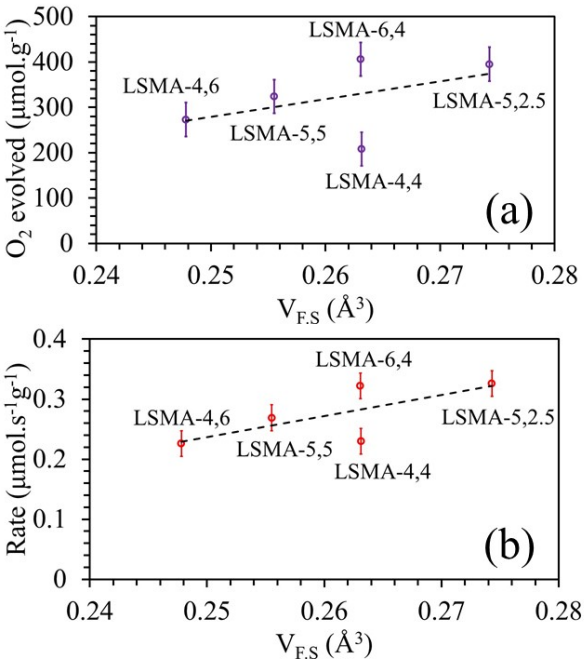

Figure S8. Amounts of O_2 evolved (a) and reduction rates (b) as a function of specific free volumes for $La_xSr_{1-x}Mn_yAl_{1-y}O_3$ oxygen carriers.

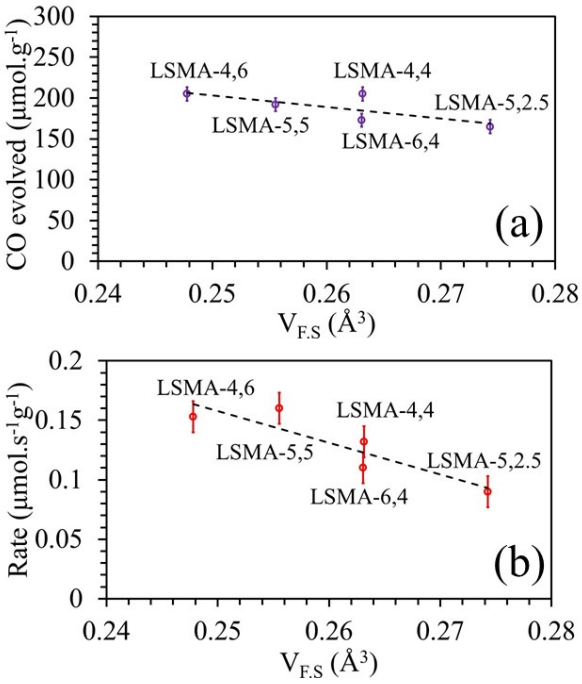

Figure S9. Amounts of CO evolved (a) and re-oxidation rates (b) as a function of specific free volumes for $La_xSr_{1-x}Mn_yAl_{1-y}O_3$ oxygen carriers.

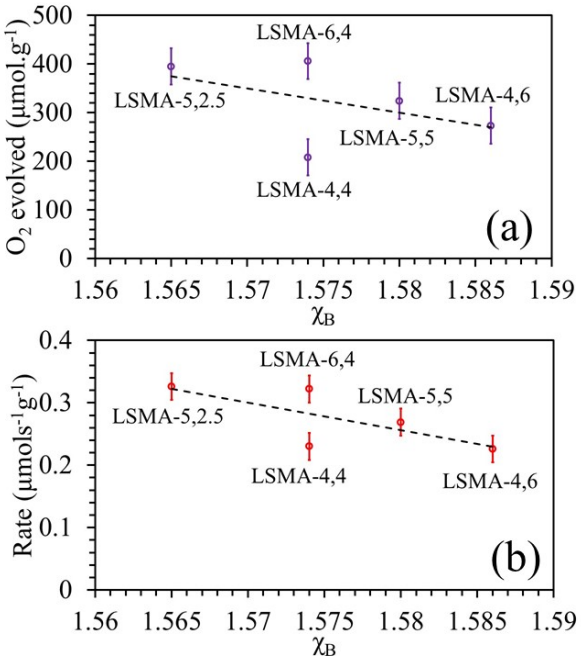

Figure S10. Amounts of O_2 evolved (a) and reduction rates (b) as a function of B-site electronegativities for $La_xSr_{1-x}Mn_yAl_{1-y}O_3$ oxygen carriers.

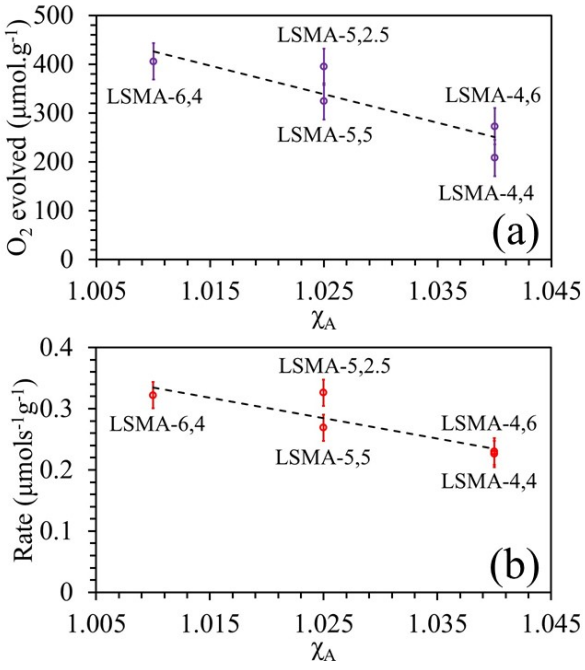

Figure S11. Amounts of O_2 evolved (a) and reduction rates (b) as a function of A-site electronegativities for $La_xSr_{1-x}Mn_yAl_{1-y}O_3$ oxygen carriers.

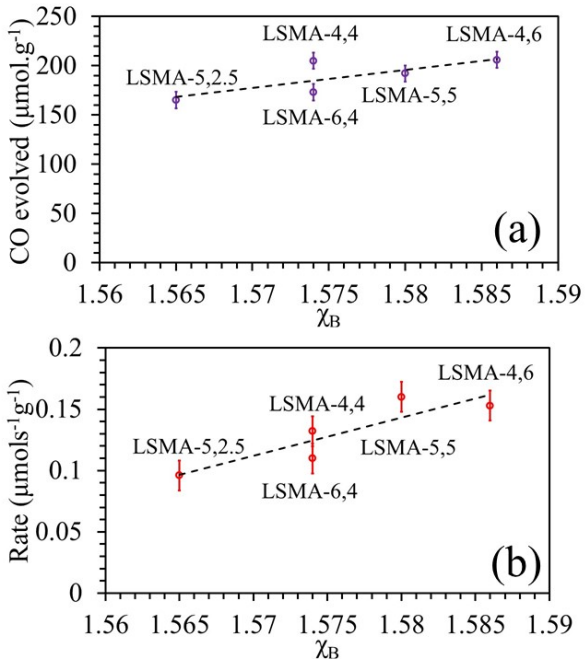

Figure S12. Amounts of CO evolved (a) and re-oxidation rates (b) as a function of B-site electronegativities for $La_xSr_{1-x}Mn_yAl_{1-y}O_3$ oxygen carriers.

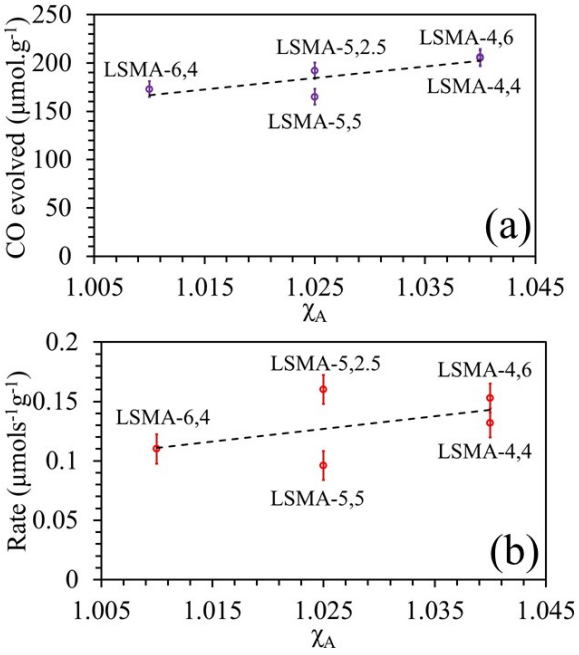

Figure S13. Amounts of CO evolved (a) and re-oxidation rates (b) as a function of A-site electronegativities for $La_xSr_{1-x}Mn_yAl_{1-y}O_3$ oxygen carriers.

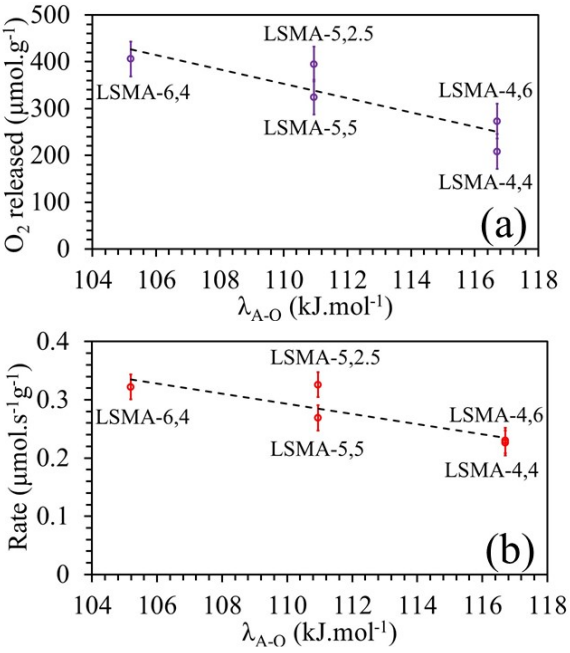

Figure S14. Amounts of O_2 evolved (a) and reduction rates (b) as a function of A-O bond energies for $La_xSr_{1-x}Mn_yAl_{1-y}O_3$ oxygen carriers.

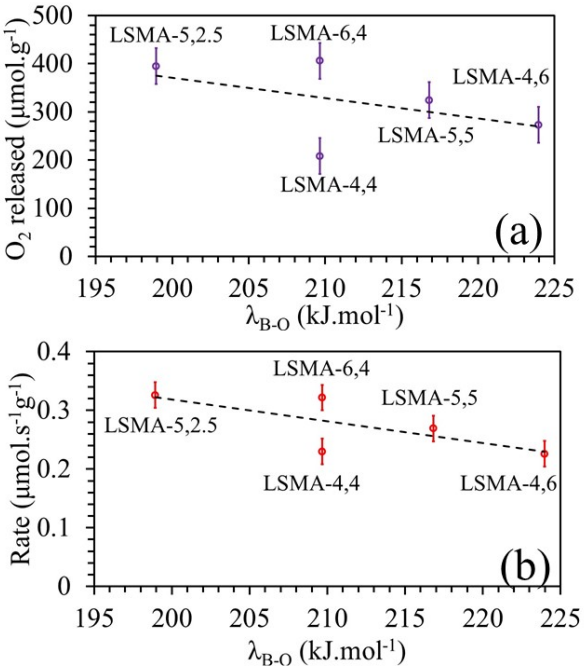

Figure S15. Amounts of O_2 evolved (a) and reduction rates (b) as a function of B-O bond energies for $La_xSr_{1-x}Mn_yAl_{1-y}O_3$ oxygen carriers.

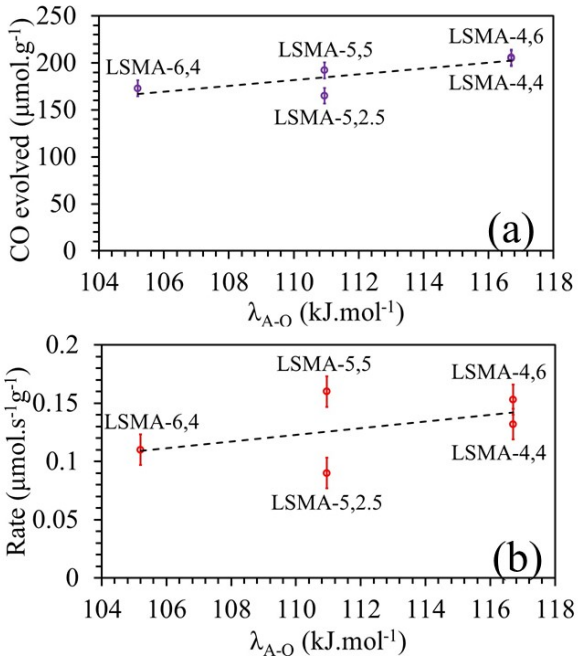

Figure S16. Amounts of CO evolved (a) and re-oxidation rates (b) as a function of A-O bond energies for a series of $La_xSr_{1-x}Mn_yAl_{1-y}O_3$ oxygen carriers.

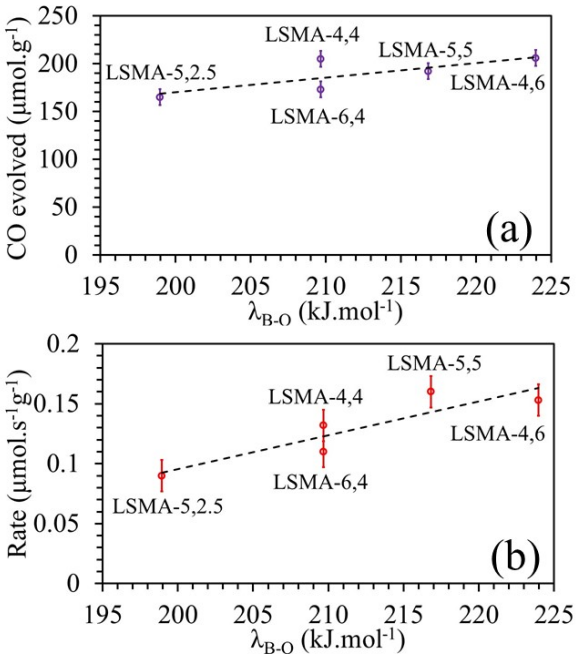

Figure S17. Amounts of CO evolved (a) and re-oxidation rates (b) as a function of B-O bond energies for a series of $La_xSr_{1-x}Mn_yAl_{1-y}O_3$ oxygen carriers.

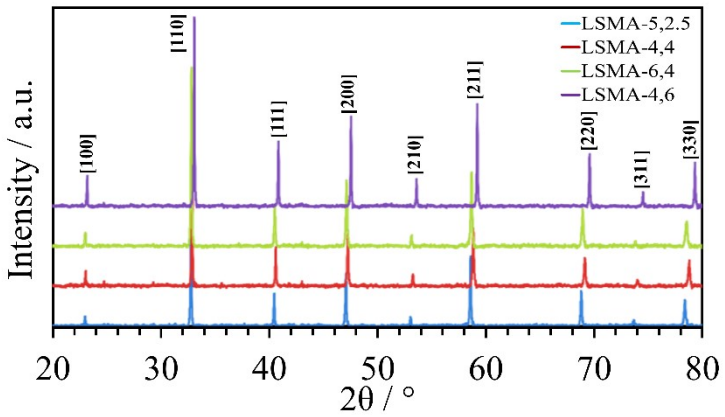

Figure S18. Wide angle powder XRD patterns observed for $La_xSr_{1-x}Mn_yAl_{1-y}O_3$ series of perovskite oxygen carriers recovered after redox cycles comprising thermochemical reduction and subsequent CO_2 splitting at 1400 °C and 1050 °C respectively.